OPEN ACCESS
IOP Publishing
Journal of Physics B: Atomic, Molecular and Optical Physics
J. Phys. B: At. Mol. Opt. Phys. **49** (2016) 123501 (12pp)
doi:10.1088/0953-4075/49/12/123501

Invited Article

Helicity-selective phase-matching and quasi-phase matching of circularly polarized high-order harmonics: towards chiral attosecond pulses

Ofer Kfir[1], Patrik Grychtol[2], Emrah Turgut[2], Ronny Knut[2], Dmitriy Zusin[2], Avner Fleischer[1,3], Eliyahu Bordo[1], Tingting Fan[2], Dimitar Popmintchev[2], Tenio Popmintchev[2], Henry Kapteyn[2], Margaret Murnane[2] and Oren Cohen[1]

[1] Solid State Institute and Physics Department, Technion, Haifa 32000, Israel
[2] Department of Physics and JILA, University of Colorado and NIST, Boulder, CO 80309, USA
[3] Department of Physics and Optical Engineering, Ort Braude College, Karmiel 21982, Israel

E-mail: ofertx@technion.ac.il and oren@technion.ac.il

Received 9 December 2015, revised 31 January 2016
Accepted for publication 24 February 2016
Published 23 May 2016

Abstract

Phase matching of circularly polarized high-order harmonics driven by counter-rotating bi-chromatic lasers was recently predicted theoretically and demonstrated experimentally. In that work, phase matching was analyzed by assuming that the total energy, spin angular momentum and linear momentum of the photons participating in the process are conserved. Here we propose a new perspective on phase matching of circularly polarized high harmonics. We derive an extended phase matching condition by requiring a new propagation matching condition between the classical vectorial bi-chromatic laser pump and harmonics fields. This allows us to include the influence of the laser pulse envelopes on phase matching. We find that the helicity dependent phase matching facilitates generation of high harmonics beams with a high degree of chirality. Indeed, we present an experimentally measured chiral spectrum that can support a train of attosecond pulses with a high degree of circular polarization. Moreover, while the degree of circularity of the most intense pulse approaches unity, all other pulses exhibit reduced circularity. This feature suggests the possibility of using a train of attosecond pulses as an isolated attosecond probe for chiral-sensitive experiments.

Keywords: circularly polarized high harmonic generation, phase matching, ultrafast chiral physics, attosecond pulses

(Some figures may appear in colour only in the online journal)

1. Introduction

Light sources based on high harmonic generation (HHG) are used for a variety of applications in ultrafast spectroscopy and high-resolution imaging of atoms, molecules, condensed matter and nano-structures [1–14]. While many schemes were

developed for controlling the spatial, temporal and spectral properties of HHG-based light sources [15–19], until recently bright (and useful) HHG radiation was largely limited to linear polarization.

The difficulty in controlling the polarization of HHG originates from the fact that high harmonics are emitted through a coherent recollision phenomenon [20–22]. An electron is first ripped from an atom or ion by a strong laser field. The electron then accelerates forth and back in the oscillating field, and finally recombines with the parent ion while emitting a high-energy photon. If the driving laser field is linearly polarized, the recollision (and recombination) probability is high since the trajectory of the electron is linear. This 'head on' recollision yields linearly polarized HHG bursts. Introducing ellipticity into the driving laser field results in the generation of elliptically polarized harmonics [23–25]. However, in this case the HHG efficiency drops drastically since the electron trajectory misses the parent ion [26]. Although many theoretical approaches have proposed paths toward generation of bright highly elliptical or circularly polarized high harmonics, the experimental progress was quite limited [27–40]. A notable method proposed to generate circularly polarized HHG from circularly polarized counter-rotating [27, 29, 30, 41] or co-rotating [42, 43] bi-chromatic laser fields. A single pioneering experimental work from 1995 reported the generation of high harmonics using this geometry with counter-rotating fields [44]. While indication for the correct selection rules was observed in that experiment, no attempt was made to measure the polarization state of the harmonics.

In 2013, Fleischer *et al* reported that the polarization of high harmonics can be fully controlled—from linear polarization, through elliptical, to circularly polarized high harmonics—without compromising the efficiency of the upconversion process [45, 46]. When high harmonics are driven by a bi-chromatic laser field in which the two spectral components (e.g. red (800 nm) and blue (400 nm)) are circularly polarized with opposite helicity [27, 44, 47], the resulting HHG spectrum consists of pairs of circularly polarized harmonics—also with opposite helicity. The exact spectral position and separation of the harmonic orders depend on the driving laser wavelengths: when the fundamental and second harmonic of Ti:sapphire are used, some harmonics rotate with the same helicity as the red pump (orders $3m + 1$ with $m = 1,\ 2,\ 3\ldots$) while other harmonics rotate with the same helicity as the blue pump (orders $3m - 1$). Harmonics $3m$ are forbidden [27, 29]. The HHG spectrum in [46] is non-chiral although it is comprised of circularly polarized harmonics. The average chirality cancels since pairs of counter-rotating circularly polarized harmonics have comparable power. In the time-domain, the HHG fields that correspond to such spectra consist of linearly polarized attosecond pulse trains, with rotating polarization axis [30, 46, 48]. Following the experimental generation of circularly polarized high harmonics [45, 46] phase matching and downstream application of circularly polarized HHG was demonstrated in the extreme UV (EUV) [47] and soft x-ray region [48], the associated motion of the electrons during their production was explored theoretically and experimentally [49], and a novel 3D attosecond metrology technique for characterizing the time-domain field associated with circularly polarized high harmonics was developed and demonstrated experimentally [50]. Other recent work generated circularly polarized high harmonics using crossed laser beams, to control the propagation direction of left and right circularly polarized HHG beams [51]. Finally, other techniques were experimentally demonstrated to yield generation of useful elliptically polarized high harmonics [52, 53].

An interesting question to consider is the degree of circular polarization of this novel light source and what factors determine it. In [47], we measured nearly ~100% degree of circularity for the $3m + 1$ harmonics. Importantly, we found that phase matching is helicity dependent and as such, it may be used for generating helically polarized attosecond pulses (it was recently discovered that the single atom physics of circularly polarized HHG from p-state atoms is also helicity dependent [54–56]). In that work, we derived the phase matching condition of the process by assuming three conservation laws for the HHG and pump photons: conservation of energy, linear momentum and spin angular momentum. The same method was used recently for phase matching of circularly polarized x-ray HHG [48]. Moreover, [48] considered the full propagation of the HHG and driving laser fields, while also including the influence of the degree of polarization of the driving laser fields, to predict the HHG pulse duration, detailed spectrum and hellicity.

In this invited paper, we explore phase matching of circularly polarized HHG driven by circularly polarized counter-rotating bi-chromatic pumps using two analytical approaches. First, we extend our previous analytical approaches which assumed conservation of energy, linear momentum and angular momentum in the exchange process between the pump (fundamental and its second harmonic) photons and the harmonic photons [47], to general bi-chromatic, circularly polarized, counter-rotating pumps [48]. Second, we derive a more general phase matching condition by requiring a new propagation matching condition between the classical vectorial field of the bi-chromatic pump and the resulting circularly polarized high harmonics. This approach allows us to identify that phase matching couples conservation of energy, linear and spin momenta. Under phase matching conditions, any two (out of the three) conservation laws inevitably yield the third one. We use the classical fields approach to explore the influence of the pulse envelopes on phase matching—a feature that cannot be captured within the first approach. Specifically, we derive conditions for full- and quasi-phase matching of circularly polarized HHG driven by a long circularly polarized pulse and a short counter-rotating pulse. Finally, we discuss the generation of phase-matched high harmonics that can support helically polarized attosecond pulses. We also present experimental spectra and show that they can support attosecond pulses with duration as short as 120 attoseconds per pulse, and degree of circular polarization as high as 80%.

The paper is organized as follows: in section 2 we discuss phase matching of high harmonics driven by bi-chromatic

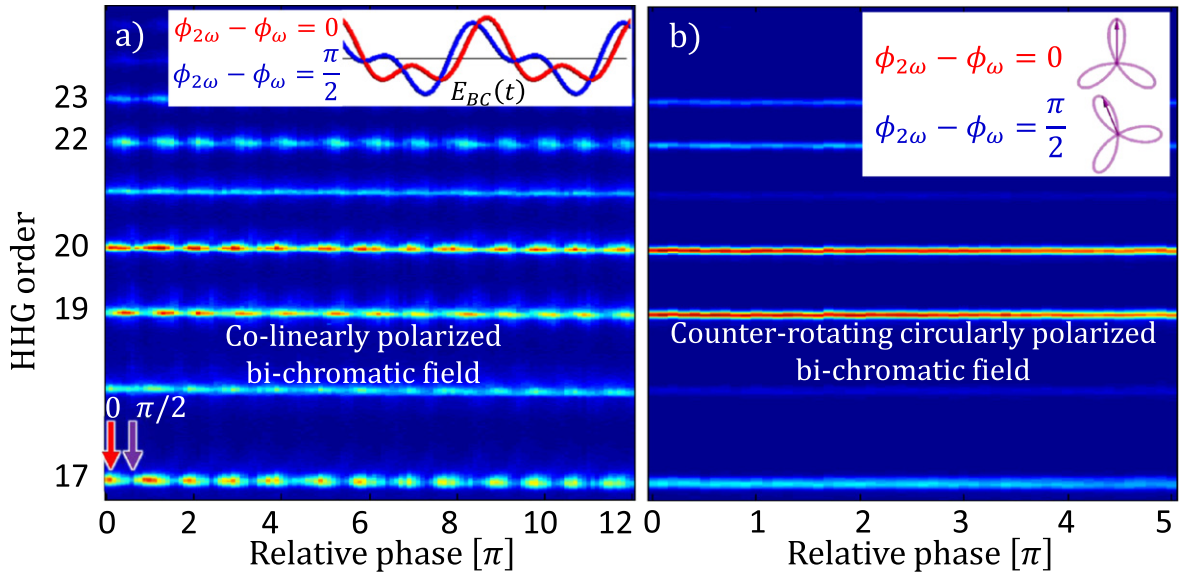

Figure 1. Experimental spectrogram of HHG pumped by a bi-chromatic field versus the relative phase between its two spectral components. (a) For a co-linear bi-chromatic pump field $\vec{E}_{\rm BC}(t) \propto \hat{x}\,\Re e\,[\exp(\mathrm{i}\omega t + \mathrm{i}\phi_\omega) + \exp(2\mathrm{i}\omega t + \mathrm{i}\phi_{2\omega})]$ the HHG spectrum oscillates with the relative phase, $\phi_{2\omega} - \phi_\omega$, since the shape of the field, $\vec{E}_{\rm BC}(t)$ is phase dependent (see inset: red curve for 0 phase and blue curve for $\pi/2$ phase). (b) HHG driven by counter-rotating circularly polarized bi-chromatic field, $\vec{E}_{\rm BC}(t) \propto \Re e\,[\hat{e}_{\rm L}\exp(\mathrm{i}\omega t + \mathrm{i}\phi_\omega) + \hat{e}_{\rm R}\exp(2\mathrm{i}\omega t + \mathrm{i}\phi_{2\omega})]$, is independent of the relative phase, $\phi_{2\omega} - \phi_\omega$, where $\hat{e}_{\rm L}$ and $\hat{e}_{\rm R}$ are left- and right-rotating circularly polarized polarizations, respectively. When varying the relative phase, the three-fold rosette shape of such a bi-chromatic field (see inset for 0 and $\pi/2$ phase) undergoes a mere rotation, which is spectrally undetectable. We associate the field shape with a Lissajous curve since the field polarization is planar, rather than a line.

pump laser fields, focusing on the difference between circularly and non-circularly polarized pump fields. Section 3 offers a concise derivation of phase matching of circularly polarized harmonics using conservation laws for photons, as derived first in [47]. In section 4 we derive the phase matching condition when treating the pump and HHG as classical quasi-monochromatic vectorial fields. We utilize the derivation of section 4 to investigate previously inaccessible regimes. As an example, we analyze phase matching regimes of circularly polarized HHG pumped by a bi-chromatic field comprised of a short pulse and a quasi-monochromatic field: the conditions for full phase matching and quasi-phase matching are analyzed in sections 5 and 6, respectively. Section 7 presents experimental highly chiral HHG spectrum and discusses the attosecond pulses that this spectrum can correspond to.

2. Polarization in full phase matching of HHG by bi-chromatic drivers

Phase matching of HHG driven by circularly-polarized bi-chromatic laser fields is very different from the case of linearly polarized lasers [47, 48]. In HHG driven by bi-chromatic linearly polarized light, the relative phase between the two spectral components of the driving field dramatically influences the phase and the intensity of the HHG field [57–59], because it changes the maximal instantaneous field and the shape of the bi-chromatic driving field. As a result, the relative phase modifies the tunnel ionization rate of the atom [60], the trajectories of these electrons in the continuum, and the resulting HHG yield [61–63]. Figure 1(a) presents the HHG spectrum as a function of the relative phase between the two colors of a co-linearly polarized bi-chromatic driving laser focused into a gas jet (see apparatus in [46]). The inset illustrates the temporal shape of the field for relative phase of 0 and $\pi/2$ between the two spectral components. When a co-linearly polarized bi-chromatic field propagates in a dispersive medium the phase of the two spectral components travel at different speeds, so their relative phase cannot be fixed. The amplitude and phase of the resulting HHG field oscillate along the propagation direction with a periodicity determined by the refractive indices of the two spectral components. The consequence of these oscillations is that full phase matching of high order harmonics is extremely challenging [64].

On the other hand, in the case of a bi-chromatic circularly polarized driving laser field, the phase between the two spectral components merely rotates the rosette-shaped field in the polarization plane (see inset of figure 1(b)). The relative phase does not change the peak intensity, nor the temporal shape of a pump field and not the resulting HHG spectrum. Figure 1(b) presents a spectrogram of HHG driven by a counter-rotating bi-chromatic pump field (see apparatus in [46]). Clearly, the HHG spectrum is independent of the relative phase between the pump spectral components. In this respect, phase matching of circularly polarized HHG driven by a circularly polarized pump is similar to phase matching of circularly polarized harmonic generation driven by a linearly polarized laser rotating in an optically active medium

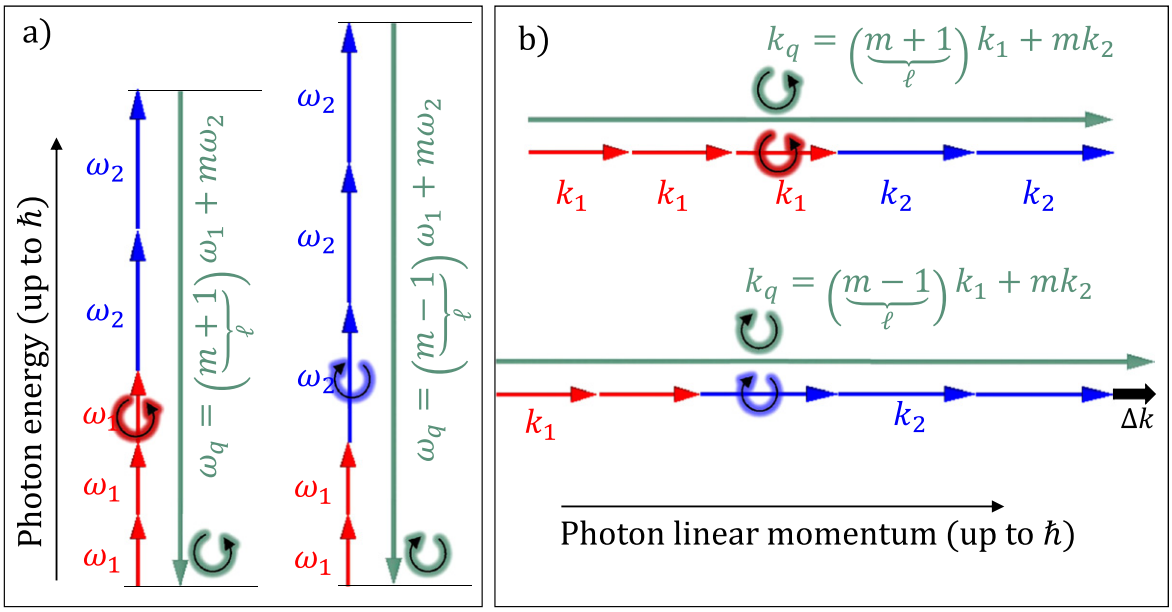

Figure 2. Conservation of energy, spin angular momentum and linear momentum in the upconversion of many circularly polarized ω_1 and ω_2 photons into a HHG photon in the qth harmonic order, ω_q. (a) HHG orders $\omega_q = (m \pm 1)\omega_1 + m\omega_2$ conserve odd parity, spin-angular momentum and energy. The emitted HHG photon inherits the spin of the extra pump photon (extra ω_1 marked red and extra ω_2 marked blue). (b) The upconversion process in a dispersive medium is helicity selective—if one helicity is phase matched, the phase of the opposite helicity is mismatched (marked by Δk).

[33, 65]. In both cases, the driving field rotates during propagation, yet its shape and amplitude are conserved. Notably, the fact that the phase of circular HHG is relatively insensitive to intensity variations (compared to linear HHG) [30] makes it more robust to pulse envelop effects and beam focusing dynamics.

3. Full phase matching condition from photon conservation laws

Below, we generalize the derivation of the phase matching equation in [47] to the case of any bi-chromatic pump; not necessarily a fundamental and its second harmonic, as was recently experimentally demonstrated for soft x-ray HHG driven by 1300 nm and 800 nm circularly-polarized lasers [48]. This section addresses the case where the pulses are long, so temporal variations in their envelope can be neglected. When HHG is driven by a bi-chromatic field composed of co-propagating left- and right-rotating circularly polarized fields, of frequency ω_1 and ω_2, respectively, the photons conservation laws are given by:

$$\text{energy} \quad \omega_q = \ell\omega_1 + m\omega_2, \tag{1}$$

$$\text{spin angular momentum} \quad \ell = m \pm 1, \tag{2}$$

$$\text{linear momentum} \quad k_q = \ell k_1 + m k_2, \tag{3}$$

ℓ and m are the number of ω_1 and ω_2 photons annihilated, respectively, from the bi-chromatic pump to generate a HHG photon at the harmonic order q with frequency $\omega_q = q\omega_1$. If ω_2/ω_1 is an integer, so is q. The HHG photon, ω_q, inherits the spin of the one extra photon it acquired, and is therefore, left-rotating for $\ell = m + 1$ and right-rotating for $\ell = m - 1$. The conservation of energy and spin angular momentum are illustrated in figure 2(a). The momentum of an HHG photon, k_q, (the factor of $\hbar$ is ommited) originates from annihilation of ℓ photons with momentum k_1 and m photons with momentum k_2 (equation (3)). Conservation of linear momentum is the condition for phase matching of circularly polarized harmonics; the HHG process is fully phase matched when equation (3) is fulfilled. However, due to chromatic and plasma dispersion in the generating medium, the fields at ω_1 and ω_2 have different refractive indices so $k_2 / k_1 \neq \omega_2/\omega_1$. The momentum mismatch (also called phase mismatch), Δk, is retrieved from equations (1), (2) and (3) to be

$$\Delta k = \ell k_1 + m k_2 - k_q = \ell\frac{\omega_1}{c}\Delta n_1 + m\frac{\omega_2}{c}\Delta n_2. \tag{4}$$

Here Δk is the phase mismatch of HHG with frequency $\omega_q = \ell\omega_1 + m\omega_2$, where $\ell = m \pm 1$. The refraction terms $\Delta n_{1,2}$ are given by $\Delta n_{1,2} = (n_{1,2} - n_q)$, where $n_{1,2}$ is the index of refraction including plasma, modal or Gouy phase terms of the pumps ω_1 and ω_2, respectively [66, 67], and n_q is the index of refraction for the harmonic order q. The condition for full phase matching is:

$$\frac{\omega_2\Delta n_2}{\omega_1\Delta n_1} = -\frac{\ell}{m} = -\frac{(m \pm 1)}{m}. \tag{5}$$

According to equation (5), Δn_2 and Δn_1 should have opposite signs. Equations (3)–(5) lead to several conclusions: First, only one HHG order can be fully phase matched for given dispersion terms $\Delta n_{1,2}$. Let us assume that the phase matched harmonic rotates like the ω_1 field. Other co-rotating

HHG orders (i.e. orders $\ell = m + 1$) differ by a small momentum addition $c^{-1}(\omega_1\Delta n_1 + \omega_2\Delta n_2)$, where the phase mismatch grows for HHG orders further away from the fully phase matched HHG order. Note that the term $(\omega_1\Delta n_1 + \omega_2\Delta n_2)$ is small since Δn_1 and Δn_2 have opposite signs. Third, all counter-rotating HHG orders ($\ell = m - 1$) have a larger phase mismatch than the co-rotating HHG orders. When compared with the phase matched HHG order, HHG orders with opposite helicity lack two ω_1 photons so their phase mismatch is approximately $\Delta k \approx 2c^{-1}\omega_1\Delta n_1$. Indeed, usually $\omega_1\Delta n_1 \gg (\omega_1\Delta n_1 + \omega_2\Delta n_2)$ so co-rotating harmonics are better phase matched than counter-rotating orders. Figure 2(b) illustrates the helicity selectiveness of such a phase matching scheme where left-rotating HHG is phase matched and right-rotating HHG exhibits a large phase mismatch (see also figure 1 in [47]).

The use of conservation laws in the above derivation implicitly utilizes continuous symmetries of the system in an intuitive way. The reliance of the phase matching equation on conservation of energy, linear momentum and angular momentum indicates that the system (light and isotropic matter) is invariant to temporal delays, spatial translations and rotations, respectively. However, one can address the system's symmetries directly. In the next section, we derive the phase matching equation using symmetries of the classical pump field propagating in an isotropic medium and retrieve the same phase matching condition as in this section, i.e. equation (4).

4. Full phase matching condition by vectorial fields symmetries.

In this section, we derive the condition for full phase matching by analyzing the operator that propagates the vectorial pump field in circularly polarized HHG (we assume nothing about the details of HHG or about the photons that participate in the process). As will be shown in this and in following sections, this formalism is much more general than the photon conservation laws approach. To derive the condition for phase matching, we identify a unitary propagator for the bi-chromatic pump in a chromatically dispersive medium and find the condition for which the emitted HHG field builds up coherently throughout the entire generation medium. Notably, unlike phase matching of linearly polarized HHG, where pump and HHG fields have the same polarization, here the fields cannot be represented by complex-valued scalars. Our description accounts for the vectorial nature of the fields.

We start by assuming a bi-chromatic field, composed of circularly polarized, counter-rotating components at frequencies ω_1 and ω_2 that propagates along z direction in an isotropic medium. For simplicity, we neglect diffraction and solve for time and propagation axes and assume plane wave propagation. We define $z = 0$ in an arbitrary position. The bi-chromatic field, $\vec{E}_{\rm BC}$, at $z = 0$ is given by:

$$\vec{E}_{\rm BC}(\tau, z = 0) = \Re e\left[\frac{E_1}{\sqrt{2}}\begin{pmatrix}1\\ \mathrm{i}\end{pmatrix}\mathrm{e}^{\mathrm{i}\omega_1\tau} + \frac{E_2}{\sqrt{2}}\begin{pmatrix}1\\ -\mathrm{i}\end{pmatrix}\mathrm{e}^{\mathrm{i}\omega_2\tau}\right]. \tag{6}$$

Here E_1 and E_2 are scalar complex amplitudes of the two spectral components of the bi-chromatic field. The 2×1 vector is the projection of the electric field on axes x and y in the polarization plane. τ represents time shifts relative to a mathematical frame of reference traveling at the phase velocity of ω_q, $v_q = c/n_q$, where c is the speed of light, so $\tau = t - n_q z/c$. This becomes useful when we look for a coherent buildup of harmonic order q—by using τ instead of t, the phase of a traveling HHG field is z-independent. For a propagating bi-chromatic field, the phase term, $\mathrm{e}^{\mathrm{i}\omega_{1,2}t - \mathrm{i}k_{1,2}z\cdot n_{1,2}}$, takes the form $\mathrm{e}^{\mathrm{i}\omega_{1,2}\tau - \mathrm{i}k_{1,2}z\cdot\Delta n_{1,2}}$ when we use τ, where $k_{1,2} = \omega_{1,2}/c$ and $\Delta n_{1,2} = n_{1,2} - n_q$. Therefore, the bi-chromatic field at $z > 0$ is

$$\vec{E}_{\rm BC}(\tau, z) = \Re e\left[\frac{E_1}{\sqrt{2}}\begin{pmatrix}1\\ \mathrm{i}\end{pmatrix}\mathrm{e}^{\mathrm{i}\omega_1\tau - \mathrm{i}\frac{\omega_1}{c}z\Delta n_1} + \frac{E_2}{\sqrt{2}}\begin{pmatrix}1\\ -\mathrm{i}\end{pmatrix}\mathrm{e}^{\mathrm{i}\omega_2\tau - \mathrm{i}\frac{\omega_2}{c}z\Delta n_2}\right]. \tag{7}$$

Note that the dispersion terms $n_{1,2}$ may include nonlinear contributions (e.g. Kerr and self-generated plasma) as long as the field intensity is constant throughout propagation. It is instructive to obtain the propagation operator that transfer $\vec{E}_{\rm BC}(\tau, 0)$ of equation (6) to $\vec{E}_{\rm BC}(\tau, z)$ of equation (7). To do so, we rearrange the exponential arguments for ω_1 and ω_2, as $\omega_1(\tau + \bar{t}) + \delta$ and $\omega_2(\tau + \bar{t}) - \delta$, respectively, and find the proper $\bar{t}$, δ

$$\bar{t}(z) = -\frac{z}{c}\frac{(\omega_1\Delta n_1 + \omega_2\Delta n_2)}{(\omega_1 + \omega_2)}, \tag{8}$$

$$\delta(z) = -\frac{z}{c}\frac{\omega_1\omega_2}{\omega_1 + \omega_2}(n_1 - n_2). \tag{9}$$

Using $\bar{t}$ and δ (equations (8) and (9)) in equation (7) leads to:

$$\vec{E}_{\rm BC}(\tau, z) = \mathrm{e}^{\bar{t}(z)\frac{\partial}{\partial\tau}}R_{\delta(z)}\vec{E}_{\rm BC}(\tau, 0). \tag{10}$$

Here $\mathrm{e}^{\bar{t}\frac{\partial}{\partial\tau}}$ is a unitary time delay operator and R_δ is the unitary rotation matrix in the polarization plane given by

$$R_\delta = \begin{pmatrix}\cos\delta(z) & \sin\delta(z)\\ -\sin\delta(z) & \cos\delta(z)\end{pmatrix}. \tag{11}$$

The time delay, $\bar{t}$, can be thought of as resulting from an effective refractive index of the bi-chromatic field, $\bar{t} = -(z/c)\Delta n^{\rm BC}_{\rm effective}$, where $\Delta n^{\rm BC}_{\rm effective}$ is a weighted average of $\Delta n_{1,2}$ with $\omega_{1,2}$ as weights.

In HHG, a process is fully phase matched if emissions from any two propagation distances interfere constructively, regardless of the propagation distance, Δz, between them. Since the bi-chromatic pump field driving the HHG emission merely rotates and delays as it propagates, the HHG fields

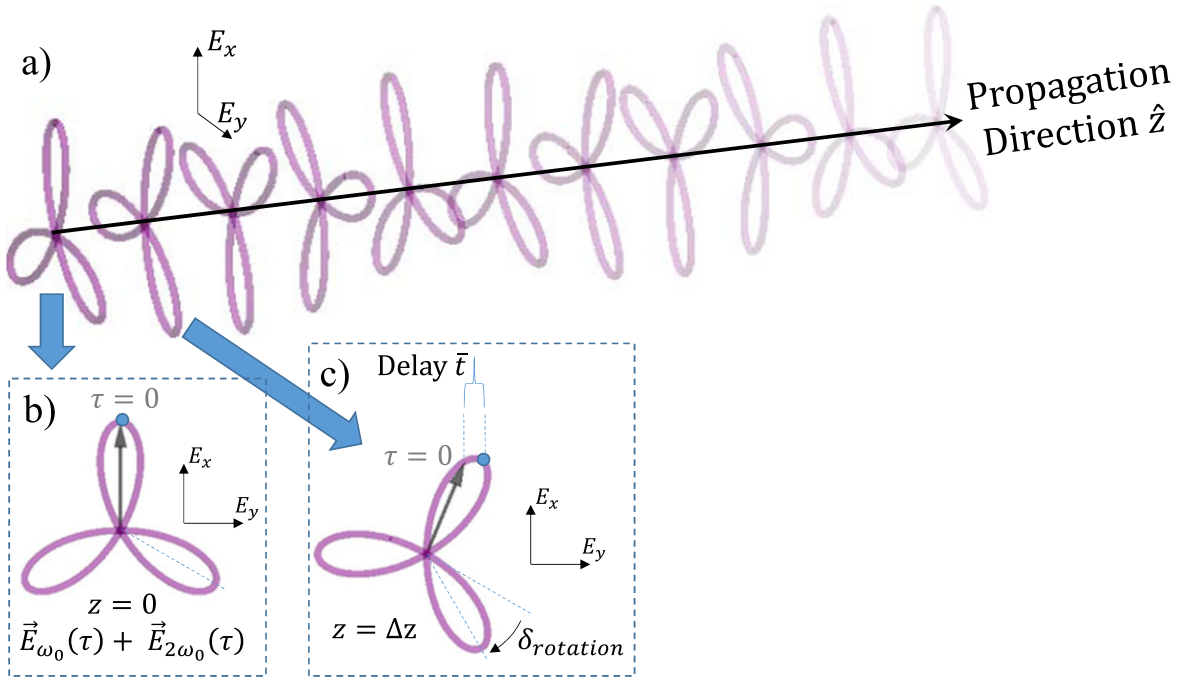

Figure 3. Propagation of a 'rosette Lissajous curve' of a bi-chromatic pump field with frequencies ω_1 and $\omega_2 = 2\omega_1$. Due to a difference in the indices of refraction for ω_1 and ω_2, the rosette shape rotates as it propagates. Insets (b) and (c) show the difference in the rosette rotation and time delay at two position on the propagation axis, separated by Δz. The black arrows in the insets is the electric field at $\tau = 0$. $\bar{t}$ corresponds to the delay accumulated over Δz between the rosette and HHG fields due to their different phase velocities. Circularly polarized HHG are fully phase matched when the phase differences induced by the time delay and by the rotation of the bi-chromatic pump, $\bar{t}$ and δ_{rotation}, respectively, exactly counteract each other. Under such a balance, the HHG emitted throughout the propagation builds up coherently. The screw-like propagation of the bi-chromatic field is a visual demonstration for the break of chiral symmetry, which is required for helicity selective HHG.

emitted at different positions are identical up to a rotation angle (same rotation angle as the driver field) and time delay. Thus, for full phase matching of q-order harmonic field generation, the net effect of the rotation and time delay should yield the identity operation (see figure 3):

$$\vec{E}_q e^{i\omega_q \tau} = \left(e^{\bar{t}(\Delta z)\frac{\partial}{\partial \tau}} R_{\delta(\Delta z)}\right)\vec{E}_q e^{i\omega_q \tau}. \tag{12}$$

Conveniently, the use of τ instead of t eliminates any explicit z-dependency of the HHG field. Equation (12) is a simple eigenvalue equation. Its solutions are the polarization eigenvectors $\vec{E}_q = \begin{pmatrix} 1 \\ \pm i \end{pmatrix}$, that correspond to left-rotating (+) and right-rotating (−) circular polarization, with eigenvalues $e^{i\omega_q \bar{t} \pm i\delta}$, respectively. Therefore, the phase matching equation condition for ω_q is

$$\omega_q \bar{t} \pm \delta = 0, \tag{13}$$

where $\bar{t}$ and δ are defined in equations (8) and (9). The phase matching equation (13) can be written explicitly as

$$0 = \frac{1}{c(\omega_1 + \omega_2)}[\omega_q(\omega_1 \Delta n_1 + \omega_2 \Delta n_2) \pm \omega_1 \omega_2 (\Delta n_1 - \Delta n_2)]. \tag{14}$$

Equations (12)–(14) correspond to the case of full phase matching. It is also instructive to formulate the phase-mismatch situation. In this case, we add a phase mismatch term, $e^{-i\Delta k \Delta z}$, to equation (12) and obtain: $\vec{E}_q e^{i\omega_q \tau - i\Delta k \Delta z} = e^{\bar{t}(\Delta z)\frac{\partial}{\partial \tau}} R_{\delta(\Delta z)} \vec{E}_q e^{i\omega_q \tau}$. Hence, the phase mismatch generalization to equation (14) is given by:

$$\frac{\pi}{L_c} = \Delta k = \frac{1}{c(\omega_1 + \omega_2)}[\omega_q(\omega_1 \Delta n_1 + \omega_2 \Delta n_2) \pm \omega_1 \omega_2 (\Delta n_1 - \Delta n_2)], \tag{15}$$

where L_c is the coherence length of the conversion process.

Thus far we derived two different equations for phase matching of circularly polarized HHG driven by bi-chromatic circularly polarized counter-rotating drivers: equations (4) and (15). Equation (15) is more general as it does not require to 'count' the number of annihilated photons, ℓ and m, as input parameters. The two equations coalesce if one assumes any two out of the three conservation laws (equations (1), (2) or (3)). For example, equation (3) can be derived directly from equations (15), (1) and (2). In a similar fashion, equation (2) can be derived from equations (15), (1) and (3). This feature reveals that the phase matching in our scheme couples the conservation laws for the photons in the process.

Figure 3 illustrates the propagation effects on a circularly polarized counter-rotating bi-chromatic field comprising a fundamental field, ω_1, and its second harmonic, $\omega_2 = 2\omega_1$. As the field travels in a chromatically dispersive medium, the three-fold rosette shape of the field rotates since ω_1 and ω_2 acquire a phase shift (figure 3(a)). This screw-like propagation

clearly shows that the pump is chiral, and therefore, one should expect a major difference in the coherence lengths of high harmonics with left helicity versus right helicity. Circularly polarized fields are a unique outcome for such a screw-like propagation since spatial rotation simply induce a phase [33, 49, 65]. According to equation (13), the HHG phase is matched when the chirally selective phase of the spatial rotation, δ, balances the time delay phase, the result should be $\omega_q \bar{t}$, which is a non-chiral effect of the propagation. Figures 3(b) and (c) show δ and $\bar{t}$ for two positions along the propagation axis, $z = 0$ and $z = \Delta z$. Notably, while figure 3 illustrates the balance between the time delay and rotation for the case of $\omega_2 = 2\omega_1$, it works for any $\omega_1 \neq \omega_2$.

5. Full phase matching of circularly polarized HHG by a short and a long pump pulses

In the previous sections, we derived the phase matching equation while neglecting the envelopes of the bi-chromatic pump pulses. In this section we extend the analysis to include the effect of pulse envelope. Specifically, we shall discuss full phase matching conditions for circularly polarized HHG pumped by a combination of a short circularly polarized pulse at ω_1 and a long counter-rotating pulse at ω_2 [54]. The properties of the HHG formed by such a pump field depend strongly on the carrier-envelope phase, that is, the time difference between the pulse envelope and the peak of the oscillating field. Models based on continuous symmetries or conservation laws for photons (e.g. the model in section 3) neglect this dependence and are therefore incomplete. The vectorial fields model (section 4), on the other hand, can be extended to include the effect of the pulse envelope.

In short, if the velocities of the envelope and the peak of the carrier bi-chromatic field are equal (although the carrier field might rotate), then the shape of the field is independent of the propagation. In this case, high harmonics that propagate with the same velocity would be fully phase matched. If, on the other hand, the velocities of the envelope and carrier field differ, then the field's shape oscillates as it propagates through the medium, and the HHG field may only be quasi phase matched (see section 6). In this and the following section the vectorial nature of the pump field is addressed explicitly and accounts for variations of orientation, amplitude and phase of the electric field throughout propagation. For simplicity, we take into account the group and phase velocities of the pump fields but leave out higher order effects such as group velocity dispersion, and effects of ionization within the duration of the short pump pulse.

We assume that the bi-chromatic field, $\vec{E}^{\,\mathrm{p}}_{\mathrm{BC}}$, entering the medium at $z = 0$ is given by:

$$\vec{E}^{\,\mathrm{p}}_{\mathrm{BC}}(\tau, 0) = \Re e\left[\frac{E_1}{\sqrt{2}}\begin{pmatrix}1\\ \mathrm{i}\end{pmatrix} e^{\mathrm{i}\omega_1\tau - \frac{\tau^2}{2\sigma_t^2}} + \frac{E_2}{\sqrt{2}}\begin{pmatrix}1\\ -\mathrm{i}\end{pmatrix} e^{\mathrm{i}\omega_2\tau}\right]. \tag{16}$$

The field at frequency ω_1 is confined to a Gaussian envelope with a standard deviation σ_t, and the pulse duration of the field at ω_2 is much longer and is taken as infinite. Here we marked the bi-chromatic field with a superscript 'p' to denote the pulsed nature of the field and to distinguish it from the bi-chromatic fields in previous sections. The pulse envelop is taken as Gaussian for simplicity, however, the derivation is general and can be applied to any pulse envelope. Due to propagation of distance z in the medium, the field undergoes chromatic dispersion (similar to equation (7)) while the pulse envelope aquires a group delay z/v_{g}, so

$$\vec{E}^{\,\mathrm{p}}_{\mathrm{BC}}(\tau, z) = \Re e\left[\frac{E_1}{\sqrt{2}}\begin{pmatrix}1\\ \mathrm{i}\end{pmatrix} e^{\mathrm{i}\omega_1\tau - \mathrm{i}k_1 z\,\Delta n_1 - \frac{1}{2\sigma_t^2}\left(\tau - z\left(\frac{1}{v_{\mathrm{g}}} - \frac{1}{v_q}\right)\right)^2} + \frac{E_2}{\sqrt{2}}\begin{pmatrix}1\\ -\mathrm{i}\end{pmatrix} e^{\mathrm{i}\omega_2\tau - \mathrm{i}k_2 z\,\Delta n_2}\right]. \tag{17}$$

v_{g} is the group velocity of a pulse centered at ω_1 and we substituted $\tau = t - z/v_q$, and $\Delta n_{1,2} = (n_{1,2} - n_q)$. With the same logic as in section 4, we wish to extract the symmetry propagator that links $\vec{E}^{\,\mathrm{p}}_{\mathrm{BC}}(\tau, 0)$ and $\vec{E}^{\,\mathrm{p}}_{\mathrm{BC}}(\tau, z)$. We claim that the HHG phase is matched when the field of the HHG order q conforms to the same propagator. We start by extracting the time and rotation operators, $e^{\bar{t}(z)\frac{\partial}{\partial\tau}} R_{\delta(z)}$, as in equation (10)

$$\vec{E}^{\,\mathrm{p}}_{\mathrm{BC}}(\tau, z) = e^{\bar{t}\frac{\partial}{\partial\tau}} R_\delta\, \Re e\left[\frac{E_1}{\sqrt{2}}\begin{pmatrix}1\\ \mathrm{i}\end{pmatrix} e^{\mathrm{i}\omega_1\tau - \frac{1}{2\sigma_t^2}\left(\tau - \bar{t} - z\left(\frac{1}{v_{\mathrm{g}}} - \frac{1}{v_q}\right)\right)^2} + \frac{E_2}{\sqrt{2}}\begin{pmatrix}1\\ -\mathrm{i}\end{pmatrix} e^{\mathrm{i}\omega_2\tau}\right]. \tag{18}$$

By using $\bar{t}$ and δ we eliminate the terms $e^{-\mathrm{i}k_{1,2}z\,\Delta n_{1,2}}$ but add an explicit time shift, $\bar{t}$, to the pulse envelope. For the operator to be unitary, as in equation (12), equation (13) should hold and also the term $\bar{t} + z\left(\frac{1}{v_{\mathrm{g}}} - \frac{1}{v_q}\right)$ should nullify, leading to the condition

$$0 = \bar{t} + z\left(\frac{1}{v_{\mathrm{g}}} - \frac{1}{v_q}\right) = z\left[-\frac{1}{c}\frac{(\omega_1\Delta n_1 + \omega_2\Delta n_2)}{(\omega_1 + \omega_2)} + \left(\frac{1}{v_{\mathrm{g}}} - \frac{1}{v_q}\right)\right]. \tag{19}$$

This additional condition for full phase matching cannot be predicted by considering the conservation of energy, spin angular momentum and linear momentum of the pump and HHG photons, and requires the explicit approach presented here. Equation (19) accounts for the relative time delay between the bi-chromatic field (induced by chromatic dispersion) and the group delay of the pulse envelope. When equation (19) is fulfilled and this relative time delay nullifies, the shape of the bi-chromatic field is independent throughout propagation, up to trivial time delays and rotations. The HHG field that this field produces will be identical along propagation, up to these delays and rotation, similarly to the case described in section 4. Therefore, the phase matching condition for the HHG field is equal to the condition in

equation (15), with the addition of equation (19)

$$\begin{cases} \Delta k = \dfrac{1}{c(\omega_1+\omega_2)}[\omega_q(\omega_1\Delta n_1+\omega_2\Delta n_2) \\ \qquad \pm\ \omega_1\omega_2(\Delta n_1-\Delta n_2)] \\ 0 = -\dfrac{(\omega_1\Delta n_1+\omega_2\Delta n_2)}{(\omega_1+\omega_2)}+c\left(\dfrac{1}{v_g}-\dfrac{1}{v_q}\right). \end{cases} \tag{20}$$

Although equation (20) is similar to equation (15), in a normally dispersive medium equation (20) allows phase matching only for harmonic orders with the same helicity as ω_1. In a normally dispersive medium $n_2 > n_1$, $v_q \approx c$ and $c > v_g$, so the $\pm$ sign must be $+$ in order to nullify Δk. Intuitively, full phase matching occurs only if the envelope aquires the same time delay as the rosette of the bi-chromatic field, and therefore the entire field rotates and delayes in time, without changing its shape. Note that these are indeed the dominant HHG orders in the chiral spectra that we measured in [47] (figure (4) and also in figure (4) of this work). In the next section we show that if the shape of the pumping bi-chromatic field does vary with propagation, then the HHG process can be quasi phase matched (QPM).

6. Quasi phase matching of circularly polarized HHG

In this section we consider the case where the envelope and the rosette field do not propagate with equal velocities (i.e. equation (19) is not satisfied), leading to a continuous slip between the phase and the envelope of the bi-chromatic pump. In such a case, the phase and amplitude of the emitted HHG field vary periodically as the pump propagates in the generation medium and HHG can be QPM [67], but not fully phase matched. To find the periodicity of the phase slip we use a property of counter-rotating bi-chromatic pump: a time delay of $2\pi/(\omega_1+\omega_2)$ simply rotates the field by a spatial angle $2\pi\omega_1/(\omega_1+\omega_2)$. A rotation by this angle does not change the bi-chromatic field. In the particular case of $\omega_2 = 2\omega_1$, a delay of $2\pi/3\omega_1$ (1/3 of an optical cycle) is equivalent to a rotation by 120°, which is exactly the rotation symmetry of the bi-chromatic field. Therefore, although the envelope delay term in equation (18), $\bar{t}+z(v_g^{-1}-v_q^{-1})$, may not nullify continuously, it nullifies after propagating one period, marked Λ (see notation in section 2.9 in Boyd [68]). For example, if the carrier bi-chromatic field and the envelope reach their maxima together at some position, they also reach their maxima jointly after propagating Λ, albeit with some time delay and rotation. It is convenient to define a time delay, τ_Λ, and to write its relation with Λ in the following form

$$\tau_\Lambda = \frac{2\pi}{\omega_1+\omega_2} = \bar{t}(\Lambda)+\Lambda\left(\frac{1}{v_g}-\frac{1}{v_q}\right), \tag{21}$$

where $\bar{t}$ is defined in equation (8). The right-hand side of (21) allows us to nullify the envelope delay term in equation (18), where the definition $\tau_\Lambda = 2\pi/(\omega_1+\omega_2)$ is usful for our derivation, since it takes into accout the temporal and rotational symmetries of the the bi-chromatic field.

We write the bi-chromatic field after it propagates Λ using equation (18). We employ a unitary operation that adds τ_Λ within the brackets and adds $-\tau_\Lambda$ to the time delay operator to simplify the envelope group delay term (see equation (21))

$$\vec{E}^{\,p}_{BC}(\tau,\Lambda) = e^{(\bar{t}-\tau_\Lambda)\frac{\partial}{\partial\tau}}R_\delta\Re e\left[\frac{E_1}{\sqrt{2}}\begin{pmatrix}1\\ i\end{pmatrix}e^{i\omega_1(\tau+\tau_\Lambda)-\frac{\tau^2}{2\sigma_t^2}} + \frac{E_2}{\sqrt{2}}\begin{pmatrix}1\\ -i\end{pmatrix}e^{i\omega_2(\tau+\tau_\Lambda)}\right]. \tag{22}$$

The additional delay, τ_Λ, is apparent in the phasors $e^{i\omega_{1,2}(\tau+\tau_\Lambda)}$. The definition $\tau_\Lambda = 2\pi/(\omega_1+\omega_2)$ now becomes useful, since according to the symmetries of the bi-chromatic field, a spatial rotation by $2\pi\omega_1/(\omega_1+\omega_2)$ removes τ_Λ from the phasors and retreives $\vec{E}^{\,p}_{BC}(\tau,0)$ in the square brackets. Thus, we can write a unitary discrete propagator for the bi-chromatic field, including the effects of the envelope

$$\vec{E}^{\,p}_{BC}(\tau,\Lambda) = \left(e^{(\bar{t}-\tau_\Lambda)\frac{\partial}{\partial\tau}}R_{\delta+\omega_1\tau_\Lambda}\right)\vec{E}^{\,p}_{BC}(\tau,0). \tag{23}$$

The quasi-phase matching condition for the HHG field, $\vec{E}_q$, with frequency, ω_q, can be retreived with the same logic leading to equations (12) and (15). To be QPM, the HHG field should be equal at two positions separated by distance Λ, where deviations from QPM are expressed by the phase mismatch term, Δk_Q

$$\vec{E}_q e^{i\omega_q\tau - i\Delta k_Q\Lambda} = e^{(\bar{t}-\tau_\Lambda)\frac{\partial}{\partial\tau}}R_{\delta+\omega_1\tau_\Lambda}\vec{E}_q e^{i\omega_q\tau}. \tag{24}$$

The condition for QPM is retreived by substituting circularly polarized HHG into equation (24)

$$-\Delta k_Q\Lambda + 2\pi l = (\omega_q\bar{t}(\Lambda)\pm\delta(\Lambda)) + (-\omega_q\pm\omega_1)\tau_\Lambda, \tag{25}$$

where l is an integer representing the QPM order (not to be confused with ℓ of equation (1)). We use equations (8), (9) and (15) to replace the left brackets with the phase mismatch, $-\Delta k\Lambda$, and use equation (21) to get the explicit QPM equation

$$-\Delta k_Q\Lambda + 2\pi l = -\Delta k\Lambda + 2\pi(-\omega_q\pm\omega_1)/(\omega_1+\omega_2). \tag{26}$$

By the relation $\omega_q = m(\omega_1+\omega_2)\pm\omega_1$ (equations (1) and (2)) we get a simple condition for QPM

$$\Delta k_Q = \Delta k + \frac{2\pi}{\Lambda}(l+m), \tag{27}$$

where l is order of QPM and m is related to the HHG order. Equation (27) implies that for QPM, $\Delta k_Q = 0$, the phase mismatch from the bi-chromatic carrier wave, Δk, should balance an integer order of the periodicity of the carrier envelope phase slip, $2\pi/\Lambda$. If an harmonic order with a given m is quasi-phase matched according to equation (27) with a

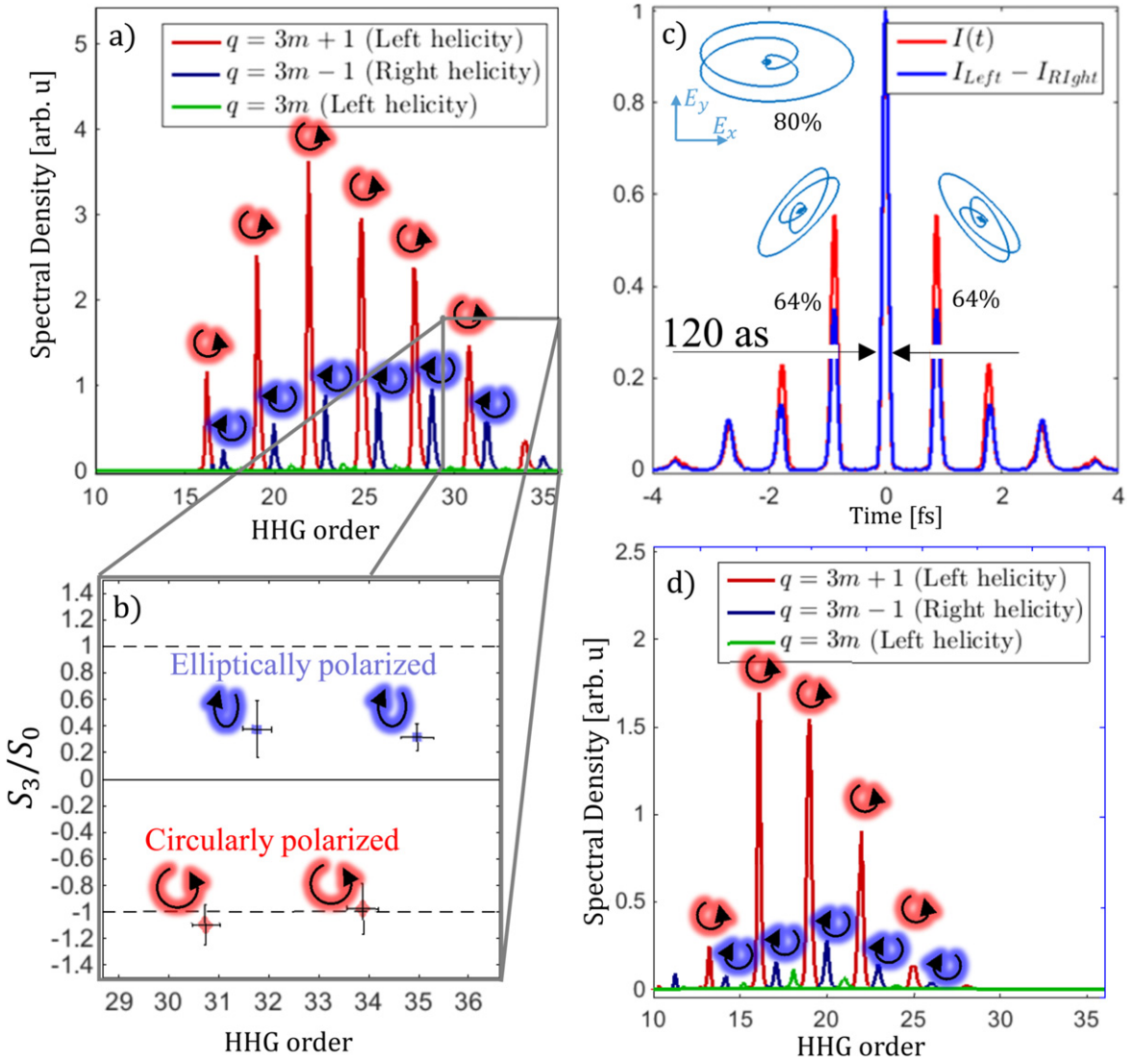

Figure 4. Highly chiral HHG and attosecond pulses. (a) Chiral spectrum recorded in gaseous neon [47], where the left-rotating HHG orders (red) dominate over the right-rotating HHG orders (blue). Furthermore, the HHG radiation acquires additional chirality since (b) the degree of circular polarization, defined as the normalized Stokes parameter S_3/S_0, is 100% for the left-rotating HHG and 40% for the right-rotating HHG (see figure S.3 in [47]). (c) In time domain, the above spectrum corresponds to a train of highly chiral attosecond bursts, supporting pulse duration as short as 120 attoseconds (red line). Interestingly, neighboring attosecond bursts have lower degree of circular polarization (noted in %). Therefore, if such emission probes a chiral phenomenon (e.g. circular dichroism), most of the chiral signal (blue line) comes from a single attosecond pulse. (d) Experimentally acquired spectrum from a waveguide full of neon gas showing extremely high selectivity for left-rotating harmonics (red) over right-rotating harmonics (blue). The extremely high chirality of such a spectrum can be directly identified from the contrast between the left- and right-rotating HHG orders. It supports a train of attosecond pulses with similar features as in (c).

given QPM order l, other HHG orders (different m, with equal or opposite helicity) may still nullify Δk_Q for a different l, however, such nullification is not guaranteed.

To conclude this section, we showed that quasi phase matching is possible, and it is helicity selective (through the $\pm$ term in Δk) similarly to full phase matching. However, it is governed by a different equation. The physical interpretation of equations (25)–(27) is more complex than for the case of full phase matching. To understand this system intuitively, consider the case where the envelope of the field at ω_1 overlaps with the peak of the bi-chromatic field, and the pulse is short enough to include only a single burst of HHG radiation. Since the group velocity of the short pulse differs from the phase velocity of the field, after some propagation distance, Λ, the pulse envelope ovelaps with an adjacent peak of the bi-chromatic field's rosette. At that point, the shape of the field is as it was originally up to a temporal delay, $\bar{t} - \tau_\Lambda$, and rotation, $\omega_1 \tau_\Lambda$. The HHG emitted from atoms separated by Λ is identical, up to the these delay and rotation. HHG is QPM if the emissions at every Λ differ by $2\pi l$ and interfere constructively.

7. Helically polarized attosecond pulses

Generation of circularly polarized high harmonics by bi-chromatic counter-rotating circularly polarized drivers results

in a comb of harmonic pairs, where in each pair the harmonics rotate in opposite directions, and can span the EUV and soft x-ray regions [46–48]. Generally, the average chirality of the field is rather small because the intensities of the left-rotating and right-rotating harmonics are comparable [46]. Thus, in order to generate helically polarized attosecond pulses, we need to, somehow, break this symmetry. We need a helicity-dependent filter. As discussed in previous sections, phase matching of circularly polarized high harmonics is strongly helically dependent [47].

In this section, we present experimentally measured spectra of circularly polarized HHG with a high degree of average chirality and show that this measured spectrum can support attosecond pulses with a large degree of circular polarization (the experimental corroboration for phase matching was presented in [47, 48]). Figure 4(a) shows a spectrum for circularly polarized HHG from neon that appears on figure 3(b) in [47]. The HHG process was driven by a ω_1 (790 nm) circularly polarized left rotating driver and its second harmonic, i.e. $\omega_2 = 2\omega_1$, which rotated in the opposite direction. In this case, the allowed harmonic orders are $q = 3m \pm 1$, where m is an integer and $q = \omega_q/\omega_1$. Harmonic orders $q = 3m + 1$ are left-rotating, as ω_1, and HHG orders $q = 3m - 1$ are right-rotating, as ω_2, where HHG orders $q = 3m$ are suppressed (marked red, blue and green, respectively, in figure 4(a)). Clearly, the left-rotating harmonic peaks are 3–5 times higher than their adjacent right-rotating peaks. Notably, we also measured the degree of circular polarization (i.e. the normalized Stokes parameter, S_3/S_0, which is the figure of merit for magnetic chiral experiments. See p 345 in [69]) of four harmonics in this spectrum (figure 4(b), taken from figure S.3 in the supplementary information of [47]). As shown in figure 4(b), the degree of circular polarization of right-rotating HHG orders are ~40%, whereas left-rotating HHG orders are ~100% circularly polarized. In short, the left-rotating part of the HHG radiation is more intense and have higher degree of circular polarization then the right-rotating part of the spectrum.

It is instructive to analyze the time domain field that can correspond to the measured spectrum (figure 4(a)) and the degree of circular polarization (figure 4(b)). Notably, the spectral phase can be tailored downstream by using thin metal films or multi-layer mirrors [70]. It is therefore informative to calculate the transform-limited field that corresponds to the measured spectrum in figure 4(a). We calculated the time domain field assuming a flat spectral phase and associate left-rotating orders with 100% circular polarization and 40% circular polarization to the right-rotating HHG orders (i.e. ellipticity of 0.21). The resulting normalized temporal intensity is shown in figure 4(c) (red solid curve). It consists of an attosecond pulse train with pulse duration of ~120 attoseconds. All the pulses in the train have the same helicity.

Importantly, adjacent attosecond pulses have different degree of circular polarization. Of course, highly chiral pulses (high level of circular polarization) contribute more to chirality-sensitive measurements than attosecond pulses with low chirality. The dashed blue line in figure 4(c) follows the instantaneous Stokes parameter S_3, which accounts for the temporal contribution of the HHG field to a chiral asymmetry measurement; field intensity multiplied by the degree of circular polarization. To plot the blue curve, we project the electromagnetic field on left- and right-rotating circular polarization and write S_3 as the normalized difference between the intensity of the left-rotating field, I_{Left}, and the right rotating field, I_{Right}. By plotting the expected chiral sensitivity, we note a new and interesting feature in attosecond science. Even though the radiation comprises a train of attosecond pulses, the contribution to the chiral asymmetry may dominantly originate from a single attosecond pulse—the most chiral pulse (to be exact, the one with the highest Stokes parameter S_3). In addition, in figure 4(c) we actually ignored contributions of the $q = 3m$ harmonic orders for this time domain analysis. In practice, the suppressed peaks are left-rotating with 30%–50% degree of circular polarization (see figure 4(b) in [47]), and therefore, may enhance the chirality sensitivity of the dominantly chiral attosecond pulse even further, with respect to adjacent attosecond pulses. Such an effectively chirality-sensitive isolated attosecond pulse may lead to the birth of chirally selective attosecond science, where the dynamics of spin, magnetism, and angular momentum is accessible with unprecedented temporal resolution. Finally, figure 4(d) presents a measured HHG spectrum (recorded in the same experiment under similar conditions as in figure 4(a)) with an even greater ratio (10 to 1) between left- and right-rotating HHG orders. We did not measure the degree of polarization for this spectrum and therefore did not analyze its corresponding time-domain field.

8. Conclusions

In this work, we explored phase matching of circularly polarized HHG pumped by a circularly polarized counter-rotating bi-chromatic field. Using two independent analytical approaches, we generalized the phase matching equation to apply for a long bi-chromatic pump field with any two spectral components, ω_1 and ω_2. In the first approach, we imposed conservation laws for the energy, momentum and angular momentum of the photons involved in the HHG process. In the second approach, we analyzed the explicit mathematical propagator of a vectorial bi-chromatic pump field propagating in an isotropic chromatically dispersive medium. We derived a new propagation equation corresponding to phase matching for vectorial fields. This vectorial propagation condition is inherently different from phase matching of linearly polarized HHG, where the pump and HHG fields have the same polarization, so phase matching considers only the scalar amplitudes and phases. We show that the propagation equation derived from the propagator of a bi-chromatic circularly polarized pump reveals a unique symmetry. It links three conservation laws for the photons (energy, linear momentum and angular momentum): one can derive the conservation of energy, linear momentum or angular momentum from the phase matching equation (derived by the vectorial propagation condition) and the two other conservation laws. We discussed the symmetry of a

system in which HHG is pumped by a long pulse and a counter-rotating short pulse. By taking into account the effects of a temporal envelope on such a pulse, we found two additional regimes for phase matching and quasi-phase matching, and showed that these regimes are also helicity selective. In the last section, we showed that the highly chiral spectrum that we observed experimentally in [47] can support chiral attosecond pulses. We expect chiral HHG [71, 72] and attosecond pulses to open numerous opportunities to observe the dynamics of chiral phenomena, like magnetism and diverse charge, spin and orbital orderings, using all-optical tools with unprecedented temporal resolution and in spectral regions unavailable to circular polarization thus far.

Acknowledgments

This work was supported by the USA–Israel Binational Science Foundation (BSF). The Technion group was supported by the Israel Science Foundation (grant no. 1225/14), the Israeli Center of Research Excellence 'Circle of Light' supported by the I-CORE Program of the Planning and Budgeting Committee and the Israel Science Foundation, and the Wolfson foundation. The JILA authors also gratefully acknowledge support from the DOE x-ray Scattering Program Award DE-SC0002002, and an AFOSR DURIP Award FA2386-12-1-3003. PG acknowledges support from the Deutsche Forschungsgemeinschaft (no. GR 4234/1-1).

References

[1] Haight R and Seidler P F 1994 High resolution atomic core level spectroscopy with laser harmonics *Appl. Phys. Lett.* **65** 517–9
[2] Bauer M, Lei C, Read K, Tobey R, Gland J, Murnane M M and Kapteyn H C 2001 Direct observation of surface chemistry using ultrafast soft-x-ray pulses *Phys. Rev. Lett.* **87** 025501
[3] Itatani J, Levesque J, Zeidler D, Niikura H, Pepin H, Kieffer J C, Corkum P B and Villeneuve D M 2004 Tomographic imaging of molecular orbitals *Nature* **432** 867–71
[4] Baker S, Robinson J S, Haworth C A, Teng H, Smith R A, Chirilă C C, Lein M, Tisch J W G and Marangos J P 2006 Probing proton dynamics in molecules on an attosecond time scale *Science* **312** 424–7
[5] Cavalieri A L *et al* 2007 Attosecond spectroscopy in condensed matter *Nature* **449** 1029–32
[6] Sandberg R L *et al* 2007 Lensless diffractive imaging using tabletop coherent high-harmonic soft-x-ray beams *Phys. Rev. Lett.* **99** 098103
[7] Miaja-Avila L, Saathoff G, Mathias S, Yin J, La-o-vorakiat C, Bauer M, Aeschlimann M, Murnane M M and Kapteyn H C 2008 Direct measurement of core-level relaxation dynamics on a surface–adsorbate system *Phys. Rev. Lett.* **101** 046101
[8] Li W, Zhou X, Lock R, Patchkovskii S, Stolow A, Kapteyn H C and Murnane M M 2008 Time-resolved dynamics in N_2O_4 probed using high harmonic generation *Science* **322** 1207–11
[9] Goulielmakis E *et al* 2010 Real-time observation of valence electron motion *Nature* **466** 739–43
[10] Seaberg M D *et al* 2011 Ultrahigh 22 nm resolution coherent diffractive imaging using a desktop 13 nm high harmonic source *Opt. Express* **19** 22470–9
[11] Mathias S *et al* 2012 Probing the timescale of the exchange interaction in a ferromagnetic alloy *Proc. Natl Acad. Sci. USA* **109** 4792–7
[12] Hoogeboom-Pot K M *et al* 2015 A new regime of nanoscale thermal transport: collective diffusion increases dissipation efficiency *Proc. Natl Acad. Sci. USA* **112** 4846–51
[13] Miao J, Ishikawa T, Robinson I K and Murnane M M 2015 Beyond crystallography: diffractive imaging using coherent x-ray light sources *Science* **348** 530–5
[14] Zhang B, Gardner D F, Seaberg M D, Shanblatt E R, Kapteyn H C, Murnane M M and Adams D E 2015 High contrast 3D imaging of surfaces near the wavelength limit using tabletop EUV ptychography *Ultramicroscopy* **158** 98–104
[15] Gariepy G, Leach J, Kim K T, Hammond T J, Frumker E, Boyd R W and Corkum P B 2014 Creating high-harmonic beams with controlled orbital angular momentum *Phys. Rev. Lett.* **113** 153901
[16] Dudovich N, Smirnova O, Levesque J, Mairesse Y, Ivanov M Y, Villeneuve D M and Corkum P B 2006 Measuring and controlling the birth of attosecond XUV pulses *Nat. Phys.* **2** 781–6
[17] Kim K T, Zhang C, Shiner A D, Kirkwood S E, Frumker E, Gariepy G, Naumov A, Villeneuve D M and Corkum P B 2013 Manipulation of quantum paths for space-time characterization of attosecond pulses *Nat. Phys.* **9** 159–63
[18] Heyl C M, Gudde J, Hofer U and L'Huillier A 2011 Spectrally resolved maker fringes in high-order harmonic generation *Phys. Rev. Lett.* **107** 033903
[19] Fleischer A 2008 Generation of higher-order harmonics upon the addition of high-frequency XUV radiation to IR radiation: generalization of the three-step model *Phys. Rev.* A **78** 053413
[20] Corkum P B 1993 Plasma perspective on strong field multiphoton ionization *Phys. Rev. Lett.* **71** 1994–7
[21] Kulander K C, Schafer K J and Krause J L 1993 Theoretical model for intense field high-order harmonic generation in rare gases *Laser Phys.* **3** 359–64
[22] Lewenstein M, Balcou P, Ivanov M Y, L'Huillier A and Corkum P B 1994 Theory of high-harmonic generation by low-frequency laser fields *Phys. Rev.* A **49** 2117–32
[23] Weihe F A, Dutta S K, Korn G, Du D, Bucksbaum P H and Shkolnikov P L 1995 Polarization of high-intensity high-harmonic generation *Phys. Rev.* A **51** R3433–6
[24] Strelkov V V, Gonoskov A A, Gonoskov I A and Ryabikin M Y 2011 Origin for ellipticity of high-order harmonics generated in atomic gases and the sublaser-cycle evolution of harmonic polarization *Phys. Rev. Lett.* **107** 043902
[25] Antoine P, Carré B, L'Huillier A and Lewenstein M 1997 Polarization of high-order harmonics *Phys. Rev.* A **55** 1314–24
[26] Möller M, Cheng Y, Khan S D, Zhao B, Zhao K, Chini M, Paulus G G and Chang Z 2012 Dependence of high-order-harmonic-generation yield on driving-laser ellipticity *Phys. Rev.* A **86** 011401
[27] Long S, Becker W and McIver J K 1995 Model calculations of polarization-dependent two-color high-harmonic generation *Phys. Rev.* A **52** 2262–78
[28] Alon O E, Averbukh V and Moiseyev N 1998 Selection rules for the high harmonic generation spectra *Phys. Rev. Lett.* **80** 3743–6
[29] Milošević D B, Becker W and Kopold R 2000 Generation of circularly polarized high-order harmonics by two-color coplanar field mixing *Phys. Rev.* A **61** 063403
[30] Milošević D B and Becker W 2000 Attosecond pulse trains with unusual nonlinear polarization *Phys. Rev.* A **62** 011403

[31] Husakou A, Kelkensberg F, Herrmann J and Vrakking M J J 2011 Polarization gating and circularly-polarized high harmonic generation using plasmonic enhancement in metal nanostructures *Opt. Express* **19** 25346–54

[32] Yuan K-J and Bandrauk A D 2011 Generation of circularly polarized attosecond pulses by intense ultrashort laser pulses from extended asymmetric molecular ions *Phys. Rev.* A **84** 023410

[33] Liu L Z, O'Keeffe K and Hooker S M 2012 Optical rotation quasi-phase-matching for circularly polarized high harmonic generation *Opt. Lett.* **37** 2415–7

[34] Fleischer A, Sidorenko P and Cohen O 2013 Generation of high-order harmonics with controllable elliptical polarization *Opt. Lett.* **38** 223–5

[35] Yuan K-J and Bandrauk A D 2012 Circularly polarized attosecond pulses from molecular high-order harmonic generation by ultrashort intense bichromatic circularly and linearly polarized laser pulses *J. Phys. B At. Mol. Opt. Phys.* **45** 074001

[36] Yuan K-J and Bandrauk A D 2013 Single circularly polarized attosecond pulse generation by intense few cycle elliptically polarized laser pulses and terahertz fields from molecular media *Phys. Rev. Lett.* **110** 023003

[37] Ruiz C, Hoffmann D J, Torres R, Chipperfield L E and Marangos J P 2009 Control of the polarization of attosecond pulses using a two-color field *New J. Phys.* **11** 113045

[38] Zhou X, Lock R, Wagner N, Li W, Kapteyn H C and Murnane M M 2009 Elliptically polarized high-order harmonic emission from molecules in linearly polarized laser fields *Phys. Rev. Lett.* **102** 073902

[39] Mairesse Y *et al* 2010 High harmonic spectroscopy of multichannel dynamics in strong-field ionization *Phys. Rev. Lett.* **104** 213601

[40] Vodungbo B *et al* 2011 Polarization control of high order harmonics in the EUV photon energy range *Opt. Express* **19** 4346–56

[41] Milošević D B and Becker W 2002 Role of long quantum orbits in high-order harmonic generation *Phys. Rev.* A **66** 063417

[42] Zuo T and Bandrauk A D 1995 High-order harmonic generation in intense laser and magnetic fields *J. Nonlinear Opt. Phys. Mater.* **04** 533–46

[43] Bandrauk A D and Lu H 2003 Controlling harmonic generation in molecules with intense laser and static magnetic fields: orientation effects *Phys. Rev.* A **68** 043408

[44] Eichmann H, Egbert A, Nolte S, Momma C, Wellegehausen B, Becker W, Long S and McIver J K 1995 Polarization-dependent high-order two-color mixing *Phys. Rev.* A **51** R3414–7

[45] Fleischer A, Sidorenko P and Cohen O 2013 High-order harmonics of bichromatic counter-rotating elliptically-polarized drivers: fully controlled polarization state and novel selection rules *OSA Tech. Dig.* **2013** QW1A.6

[46] Fleischer A, Kfir O, Diskin T, Sidorenko P and Cohen O 2014 Spin angular momentum and tunable polarization in high-harmonic generation *Nat. Photon.* **8** 543–9

[47] Kfir O *et al* 2015 Generation of bright phase-matched circularly-polarized extreme ultraviolet high harmonics *Nat. Photon.* **9** 99–105

[48] Fan T *et al* 2015 Bright circularly polarized soft x-ray high harmonics for x-ray magnetic circular dichroism *Proc. Natl Acad. Sci. USA* **112** 14206–11

[49] Mancuso C A *et al* 2015 Strong-field ionization with two-color circularly polarized laser fields *Phys. Rev.* A **91** 031402

[50] Chen C *et al* 2016 Tomographic reconstruction of circularly polarized high-harmonic fields: 3D attosecond metrology *Sci. Adv.* **2** e1501333

[51] Hickstein D D *et al* 2015 Non-collinear generation of angularly isolated circularly polarized high harmonics *Nat. Photon.* **9** 743–50

[52] Ferré A *et al* 2015 A table-top ultrashort light source in the extreme ultraviolet for circular dichroism experiments *Nat. Photon.* **9** 93–8

[53] Lambert G *et al* 2015 Towards enabling femtosecond helicity-dependent spectroscopy with high-harmonic sources *Nat. Commun.* **6**

[54] Medišauskas L, Wragg J, van der Hart H and Ivanov M Y 2015 Generating isolated elliptically polarized attosecond pulses using bichromatic counterrotating circularly polarized laser fields *Phys. Rev. Lett.* **115** 153001

[55] Milošević D B 2015 Generation of elliptically polarized attosecond pulse trains *Opt. Lett.* **40** 2381

[56] Milošević D B 2015 Circularly polarized high harmonics generated by a bicircular field from inert atomic gases in the p state: a tool for exploring chirality-sensitive processes *Phys. Rev.* A **92** 043827

[57] Andiel U, Tsakiris G D, Cormier E and Witte K 1999 High-order harmonic amplitude modulation in two-colour phase-controlled frequency mixing *Europhys. Lett.* **47** 42

[58] Kondo K, Kobayashi Y, Sagisaka A, Nabekawa Y and Watanabe S 1996 Tunneling ionization and harmonic generation in two-color fields *J. Opt. Soc. Am.* B **13** 424

[59] Frolov M V, Manakov N L, Silaev A A and Vvedenskii N V 2010 Analytic description of high-order harmonic generation by atoms in a two-color laser field *Phys. Rev.* A **81** 063407

[60] Watanabe S, Kondo K, Nabekawa Y, Sagisaka A and Kobayashi Y 1994 Two-color Phase control in tunneling ionization and harmonic generation by a strong laser field and its third harmonic *Phys. Rev. Lett.* **73** 2692–5

[61] Ishii N, Kosuge A, Hayashi T, Kanai T, Itatani J, Adachi S and Watanabe S 2008 Quantum path selection in high-harmonic generation by a phase-locked two-color field *Opt. Express* **16** 20876

[62] Figueria de Morisson Faria C, Milošević D B and Paulus G G 2000 Phase-dependent effects in bichromatic high-order harmonic generation *Phys. Rev.* A **61** 063415

[63] Raz O, Pedatzur O, Bruner B D and Dudovich N 2012 Spectral caustics in attosecond science *Nat. Photon.* **6** 170–3

[64] Cohen O, Popmintchev T, Gaudiosi D M, Murnane M M and Kapteyn H C 2007 Unified microscopic–macroscopic formulation of high-order difference-frequency mixing in plasmas *Phys. Rev. Lett.* **98** 043903

[65] Bey P P and Rabin H 1967 Coupled-wave solution of harmonic generation in an optically active medium *Phys. Rev.* **162** 794–800

[66] Popmintchev T, Chen M-C, Bahabad A, Gerrity M, Sidorenko P, Cohen O, Christov I P, Murnane M M and Kapteyn H C 2009 Phase matching of high harmonic generation in the soft and hard x-ray regions of the spectrum *Proc. Natl Acad. Sci. USA* **106** 10516–21

[67] Popmintchev T, Chen M-C, Arpin P, Murnane M M and Kapteyn H C 2010 The attosecond nonlinear optics of bright coherent x-ray generation *Nat. Photon.* **4** 822–32

[68] Boyd R W 2003 *Nonlinear Optics* 2nd edn (New York: Academic)

[69] Stöhr J and Siegmann H C 2006 *Magnetism: From Fundamentals to Nanoscale Dynamics* (Berlin: Springer)

[70] Chini M, Zhao K and Chang Z 2014 The generation, characterization and applications of broadband isolated attosecond pulses *Nat. Photon.* **8** 178–86

[71] Cireasa R *et al* 2015 Probing molecular chirality on a sub-femtosecond timescale *Nat. Phys.* **11** 654–8

[72] Smirnova O, Mairesse Y and Patchkovskii S 2015 Opportunities for chiral discrimination using high harmonic generation in tailored laser fields *J. Phys. B: At. Mol. Opt. Phys.* **48** 234005